Appl Phys B (2009) 95: 489–495
DOI 10.1007/s00340-009-3388-0

Applied Physics B
Lasers and Optics

Non-steady-state photo-EMF in nanostructured GaN and polypyrrole within porous matrices

M. Bryushinin · V. Golubev · Y. Kumzerov · D. Kurdyukov · I. Sokolov

Received: 5 November 2008 / Revised version: 24 December 2008 / Published online: 13 February 2009

Abstract We report an experimental investigation of the non-steady-state photoelectromotive force in nanostructured GaN within porous glass and polypyrrole within chrysotile asbestos. The samples are illuminated by an oscillating interference pattern created by two coherent light beams and the alternating current is detected as a response of the material. Dependences of the signal amplitude versus temporal and spatial frequencies, light intensity, and temperature are studied for two wavelengths $\lambda = 442$ and 532 nm. The conductivity of the GaN composite is measured: $\sigma = (1.1\text{–}1.6) \times 10^{-10}\ \Omega^{-1}\,\mathrm{cm}^{-1}$ ($\lambda = 442$ nm, $I_0 = 0.045\text{–}0.19\ \mathrm{W/cm}^2$, $T = 293$ K) and $\sigma = (3.5\text{–}4.6) \times 10^{-10}\ \Omega^{-1}\,\mathrm{cm}^{-1}$ ($\lambda = 532$ nm, $I_0 = 2.3\ \mathrm{W/cm}^2$, $T = 249\text{–}388$ K). The diffusion length of photocarriers in polypyrrole nanowires is also estimated: $L_\mathrm{D} = 0.18$ μm.

PACS 42.70.Nq · 73.63.-b

1 Introduction

The utilization of non-crystalline materials instead of single-crystal analogs is the new trend in modern optics and optoelectronics. Such materials are practically feasible and cheap, they can be chemically stable, and their photoelectric properties can be easily varied.

The porous media can be considered as new objects attracting great interest of specialists in solid-state physics, optics, and semiconductors. Asbestoses, ceramics, and porous glasses are typical examples of this class of materials. The nanopores in these materials with the average diameter ranging from 10 to 100 nm may be doped with almost any gas, liquid, or a liquid solution of a solid. The physical properties of fabricated structures can be different. As the result, the material may be insulating or conductive and transparent, absorbing, or reflecting. The nanoscale of the filling component advances observation of such effects as charge localization, quantum size effect, and Peierls phase transition.

There are applications and devices where semiconductors with low conductivity are required (wafers for high-power microwave transistors, X-ray detection, holographic recording including optical data storage and processing, non-destructive testing). Gallium nitride (GaN) is considered as one of the most perspective materials for such areas. Undoped GaN samples are characterized with rather high conductivity $\sigma = 1.2 \times 10^1\text{–}3.2 \times 10^2\ \Omega^{-1}\,\mathrm{cm}^{-1}$ [1, 2]. A certain success has been achieved in fabrication of insulating GaN films using hydride vapor phase epitaxy (HVPE) methods. The conductivity of those samples reaches $\sigma \sim 10^{-12}\ \Omega^{-1}\,\mathrm{cm}^{-1}$ [3]. The production of a composite material filled with nanoparticles of GaN can be considered as another way to obtain insulating samples (especially bulk ones). The analogous idea can be realized with conductive polymer materials. Among semiconducting polymers, polypyrrole is one of the most perspective materials. It is stable in air conditions and successfully applied in construction of lithium batteries, electrolytic capacitors, photoelectrochemical cells, gas and biosensors, electrochemical actuators, etc. [4].

The application of the standard methods for semiconductor characterization (see, for example, Ref. [5]) is often restricted by the space-charge formation near the blocking

M. Bryushinin (✉) · V. Golubev · Y. Kumzerov · D. Kurdyukov · I. Sokolov
A.F. Ioffe Physical Technical Institute, 194021, St. Petersburg, Russia
e-mail: mb@mail.ioffe.ru

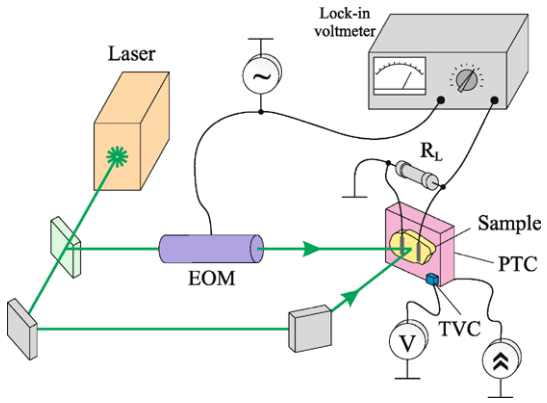

Fig. 1 Experimental setup for investigation of the non-steady-state photo-EMF in GaN nanostructure. *EOM* is the electro-optic modulator, *PTC* is the Peltier thermal converter, *TVC* is the temperature-to-voltage converter

contacts. This problem is of vital importance for investigation of high-resistive materials where space charge formation time can be very large and introduce inadmissible errors. The novel techniques based on holographic recording are more suitable for semi-insulating samples with low conductivity and mobility of photocarriers [6]. The non-steady-state photoelectromotive force (photo-EMF) technique based on the detection of the alternating electric current arising in the sample illuminated by an oscillating interference pattern is the most versatile and advanced method [7]. Since the current results from the periodic relative shifts of the photoconductivity and space-charge gratings, the technique based on this effect allows determination of the number of photoelectric parameters (conductivity, carrier sign, lifetime, diffusion length, and drift mobility) and can be applied for the investigation of both non-centrosymmetric and centrosymmetric media.

The investigation of the new class of the semi-insulating materials, namely, porous matrices filled with nanoscaled components, using the non-steady-state photo-EMF technique is the main goal of this paper.

2 Experimental setup

The experimental arrangement used for the investigation of the non-steady-state photo-EMF in porous glass filled with GaN nanoparticles is shown in Fig. 1. The light from the conventional He–Cd ($\lambda = 442$ nm, $P_{\text{out}} \simeq 3$ mW) and Nd:YAG ($\lambda = 532$ nm, $P_{\text{out}} \simeq 20$ mW) lasers was split into two beams forming the interference pattern with spatial frequency K and contrast m on the sample's surface. The signal beam was phase modulated with frequency ω and amplitude Δ by the electro-optic modulator ML-102A. The photocurrent arising in the sample generated the corresponding voltage on the load resistor $R_L = 9.1$ MΩ, which then was amplified and measured with the lock-in nanovoltmeter Unipan-232B. The experiments at $\lambda = 442$ nm were carried out at room temperature (293 K). In the experiments at $\lambda = 532$ nm we used a Peltier thermal converter and controlled the temperature by an analog temperature-to-voltage converter TC1047A.

A porous silica glass is a random structure of two interpenetrating phases, namely the solid and pore networks [8]. The pores in the glasses are connected to each other and the pore-size distribution is narrow. The structure is obtained due to spinodal decomposition of the two phases SiO_2 and $B_2O_3 + Na_2O$. After the glass is heat treated and annealed, the B_2O_3-rich phase is removed by leaching with acid, leaving an almost pure SiO_2 skeleton. The pore sizes were tested by mercury intrusion porosimetry and the average pore diameter was found to be 7 ± 1 nm. The porosity of the glass matrix was measured by a gravimetric method and it is about 30%.

Gallium nitride has been synthesized directly inside the pores by a chemical bath deposition technique similar to that described elsewhere [9]. At first, solid precursor (Ga_2O_3) was embedded into the pores of a Vycor template. We used alcohol solutions of gallium salts (gallium nitrate or gallium formate) as soluble precursors to infiltrate Ga_2O_3. The filling procedure was repeated periodically. To produce GaN the Vycor sample filled with gallium oxide was annealed in the presence of ammonia (1000 Torr) at 750°C for 50 h. The fill factor of pores with GaN was measured by a gravimetric method as well and has been found to be 25%. So, the total filling degree of the matrix by GaN is only 7–8%.

The composition of the chrysotile asbestos is $Mg_3Si_2O_5(OH)_4$. It is a regular array of closely packed, parallel, ultra-thin dielectric nanotubes. The mineral structure is described as a layer of partially hydrated MgO, which is bonded to a corresponding SiO_2 layer. Since the lattice constant in the MgO monolayer differs from that of the SiO_2 layer, this double layer rolls up in very thin tubes, with the outermost magnesium oxide layer. The fibers are therefore hollow cylindrical tubes with the outer diameter of 20–40 nm and the inner diameter of 2–10 nm [10, 11] that are convenient for nanowire preparation.

The preparation of polypyrrole nanostructures in chrysotile asbestos nanotubes was achieved by infilling them with solutions of monomers and further polymerization inside. The bulk samples of white asbestos (these are the asbestos without iron doping) with average internal diameter of nanotubes of 5 nm are used. Asbestoses were, first, stored in $FeCl_3$ solution for several days. Then, after washing in alcohol and drying, the samples were exposed to the pyrrole vapor. After pyrrole polymerization, the sample appearance changed from white to dark gray color.

The characteristic dimensions of the sample with nanostructured GaN were $3 \times 2 \times 0.16$ mm^3. The front and back

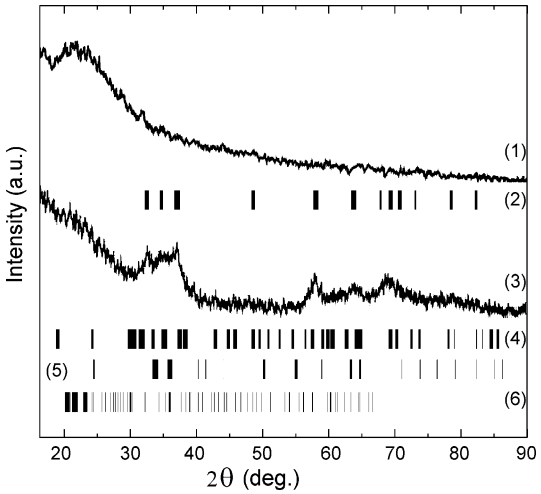

Fig. 2 X-ray diffraction patterns. *1*—bare porous glass, *2*—bulk hexagonal GaN (JCPDS 2-1078), *3*—nanocomposite porous glass–GaN, *4*—α-Ga_2O_3 (JCPDS 6-0503), *5*—β-Ga_2O_3 (JCPDS 11-370), *6*—α-tridymite (JCPDS 18-1170)

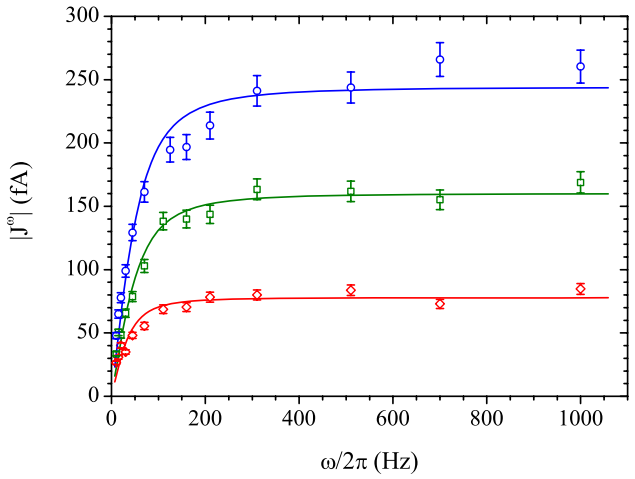

Fig. 3 Frequency transfer functions of the non-steady-state photo-EMF measured in GaN nanostructure for different light intensities: $I_0 = 0.045$ W/cm^2 (◇), 0.12 W/cm^2 (□), 0.19 W/cm^2 (○). $\lambda = 442$ nm, $K = 7.4 \times 10^4$ cm^{-1}, $m = 0.87$, $\Delta = 0.82$. The *solid lines* show the approximation by (1)

surfaces (3×2 mm^2) were polished, and the silver paste electrodes (1×1 mm^2) were painted on the front one. The characteristic dimensions of the sample with nanostructured polypyrrole were $10 \times 1 \times 0.5$ mm^3. The silver paste electrodes (1×1 mm^2) were painted on the front surface (10×1 mm^2) so that the measurements of the current along the asbestos fibers were ensured. The interelectrode spacing was 1 mm for both samples.

3 Results and discussion

The structural state of the GaN composite was determined by X-ray diffraction (XRD) measurements. The XRD patterns were obtained by using CuK_α radiation (Ni filter). Polycrystalline germanium was used as a standard. Figure 2 (curve 3) shows XRD patterns of the nanocomposite. As evident from these angular dependences of the intensities scattered, the material synthesized in the pores is the hexagonal GaN. Small amounts of crystalline phases such as α-Ga_2O_3 (JCPDS 6-0503), β-Ga_2O_3 (JCPDS 11-370), and α-tridymite (JCPDS 18-1170) were also present in the composite. The analysis of Fig. 2 (curve 3) has also provided the typical size of GaN particles: $D = 15 \pm 5$ nm. It was determined from the reflections observed at $2\Theta = 32$–$37°$ by decomposition to three Bragg peaks whose integral widths B are inversely proportional to the characteristic size of the particles: $B = \lambda_{CuK_\alpha}/D\cos\Theta$ ($\lambda_{CuK_\alpha} = 0.154$ nm). Note that this value is about two times larger than the average pore dimension. A similar feature was observed earlier in the samples of Pb within a porous glass matrix [12] and it was attributed to the elongated form of the nanoparticles.

3.1 GaN in glass matrix, $\lambda = 442$ nm

The presence of the effect of the non-steady-state photo-EMF in a new class of materials—porous glasses—is the first result that should be pointed out. In spite of the small signal amplitudes we can obtain reliable results by the use of a highly sensitive lock-in nanovoltmeter with integration time up to 100 s. We have determined the type of the photoconductivity at $\lambda = 442$ nm. The sign of the detected signal corresponds to the electronic one. The charge transport is thus assumed to be electronic rather than ionic and occurs via hopping between localized states in the glass matrix [13] (the ionic conductivity is typical for the composites containing a large proportion of ions, particularly alkali metals [14]). In our material the nanocrystals play the role of centers where electrons are optically excited and captured at deep energy levels.

The frequency transfer function of the non-steady-state photo-EMF signal amplitude is shown in Fig. 3. The signal demonstrates a typical behavior, namely, there is a linear growth of the amplitude at low frequencies of the phase modulation ω and a frequency-independent region at high frequencies. These regions are separated by the so-called cut-off frequency $\omega_0 = 48$–73 Hz. Such a behavior is an important manifestation of the adaptive nature of space-charge formation in photoconductive materials, and it is described by the following expression obtained earlier for the simplest model of the semiconductor crystal with one type of partially compensated donor centers [7]:

$$J^\omega = \frac{Sm^2\Delta\sigma_0 E_D}{2(1+K^2L_D^2)}\frac{-i\omega/\omega_0}{1+i\omega/\omega_0}, \quad (1)$$

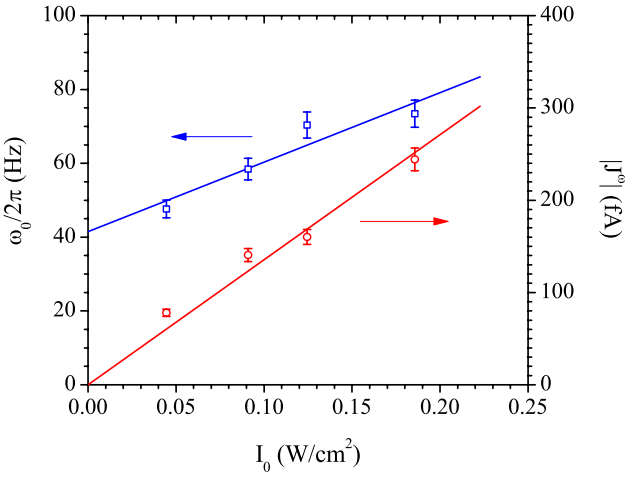

Fig. 4 Dependences of the non-steady-state photo-EMF amplitude (○) and cut-off frequency (□) on the intensity of incident light. $\lambda = 442$ nm, $K = 7.4 \times 10^4$ cm^{-1}. Both dependences are approximated by a linear function: $J^{\omega}, \omega_0 \propto I_0$

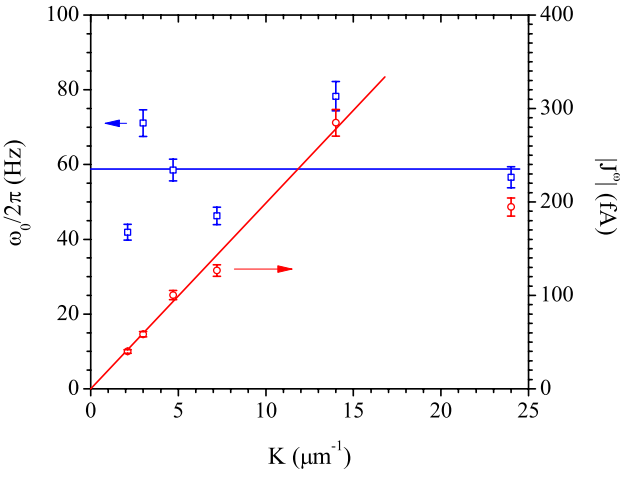

Fig. 5 Dependences of the non-steady-state photo-EMF amplitude (○) and cut-off frequency (□) on the spatial frequency of the interference pattern. $\lambda = 442$ nm, $I_0 = 0.19$ W/cm^2. The *solid lines* represent approximation by (1) and (2) for the case of small diffusion lengths $KL_D \ll 1$

with

$$\omega_0 = \left[\tau_M\left(1 + K^2 L_D^2\right)\right]^{-1}, \tag{2}$$

where S is the electrode area, σ_0 is the average photoconductivity of the crystal, $E_D = K k_B T/e$ is the diffusion field, L_D is the diffusion length of photocarriers, $\tau_M = \epsilon\epsilon_0/\sigma_0$ is the Maxwell relaxation time, T is the crystal's temperature, ϵ is the dielectric constant, ϵ_0 is the free-space permittivity, k_B is the Boltzmann constant, and e is the elementary charge.

If the light intensity increases we observe the corresponding growth of the signal amplitude (at $\omega > \omega_0$) and cut-off frequency (Fig. 4). Both dependences demonstrate an approximately linear behavior in the investigated intensity range: $J^{\omega}, \omega_0 \propto I_0$, which is due to increase of the sample's photoconductivity σ_0 [see (1) and (2)]. The method of the non-steady-state photo-EMF provides a possibility for determination of the conductivity in highly resistive materials: on measuring the cut-off frequency we can easily calculate the Maxwell relaxation time and conductivity of the sample [see (2)]. The investigated glass has $\epsilon \simeq 4$, so the conductivity equals $\sigma = (1.1\text{–}1.6)\times 10^{-10}$ Ω^{-1} cm^{-1} for $I_0 = 0.045\text{–}0.19$ W/cm^2. One can note that the cut-off frequency tends to a non-zero limit at low intensities: $\omega_d/2\pi = \lim_{I_0 \to 0} \omega_0/2\pi = 41$ Hz. It is most probably associated with the finite dark conductivity of the material, which is estimated from the value of this limit: $\sigma_d = \epsilon\epsilon_0\omega_d = 9 \times 10^{-11}$ Ω^{-1} cm^{-1}.

The dependence of the signal amplitude and cut-off frequency versus spatial frequency of the interference pattern is presented in Fig. 5. The dependence of the signal amplitude $|J^{\omega}(K)|$ seems to be linear in the range $K = 0\text{–}14$ μm^{-1}, which is due to increase of the diffusion field E_D. The sufficient deviation of the last point from the claimed linear dependence is probably caused by the increase of the light reflection and shadowing of the near-contact area but not by the blurring of the oscillating photoconductivity distribution observed at $K > L_D^{-1}$. The scattering of the cut-off frequency values is noticeable as well, and no decrease of this parameter at high spatial frequencies is guessed [see (2)]. So, we can state that the diffusion length of electrons is too small to be measured using this technique: $L_D < 40$ nm.

3.2 GaN in glass matrix, λ = 532 nm

In this subsection we consider the excitation of the non-steady-state photo-EMF signal at $\lambda = 532$ nm and consider its temperature dependence. The sign of the signal corresponds to the electron type of conductivity.

The frequency transfer functions of the non-steady-state photo-EMF measured at different temperatures are shown in Fig. 6. The signal demonstrates a behavior similar to the one at $\lambda = 442$ nm. The conductivity values derived from the cut-off frequencies are the following: $\sigma = (3.5\text{–}4.6)\times 10^{-10}$ Ω^{-1} cm^{-1} ($T = 249\text{–}388$ K). The signal amplitude and cut-off frequency are slightly higher than the ones at $\lambda = 442$ nm but this results from the much higher intensities of light, so we can state that excitation of the signal at $\lambda = 532$ nm is less effective. The following reasons for this difference can be pointed out: the material has a larger absorption coefficient at shorter wavelength ($\alpha = 440$ cm^{-1} at $\lambda = 442$ nm versus $\alpha = 280$ cm^{-1} at $\lambda = 532$ nm) and, perhaps, larger quantum efficiency of the conductivity.

The temperature dependence of the cut-off frequency is rather linear in the investigated range of temperatures $T = 249\text{–}388$ K (Fig. 7):

$$\omega_0 = A(T + T'), \tag{3}$$

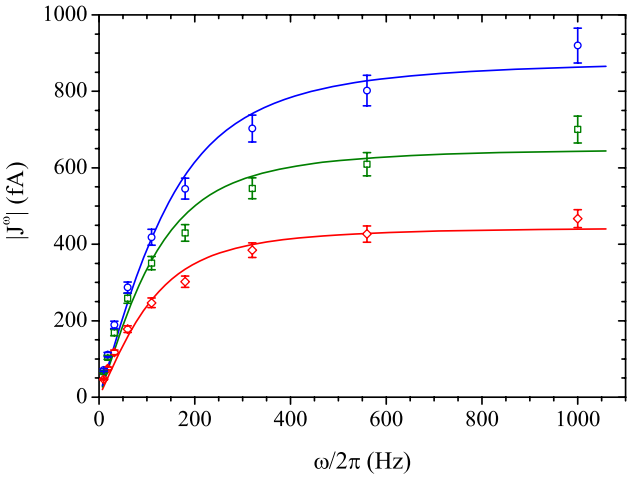

Fig. 6 Frequency transfer functions of the non-steady-state photo-EMF measured in GaN nanostructure for different temperatures: $T = 249$ K (◇), 287 K (□), 388 K (○). $\lambda = 532$ nm, $I_0 = 2.3$ W/cm^2, $K = 7.1 \times 10^4$ cm^{-1}, $m = 0.91$, $\Delta = 0.61$. The best fit of the experimental data by (1) is shown by the *solid lines*

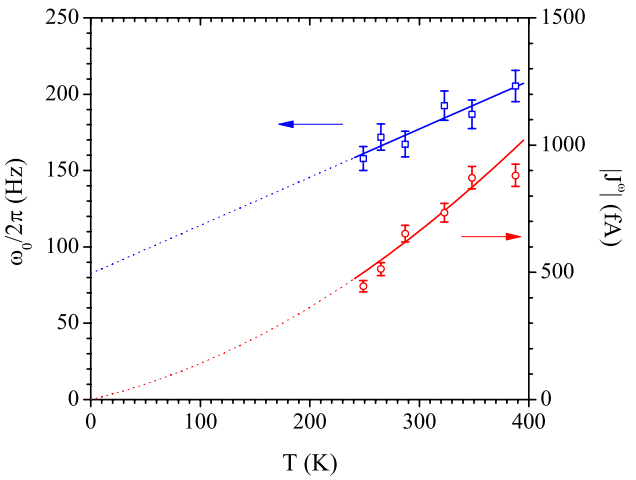

Fig. 7 Dependences of the non-steady-state photo-EMF amplitude (○) and cut-off frequency (□) on the sample's temperature. $\lambda = 532$ nm, $I_0 = 2.3$ W/cm^2, $K = 7.1 \times 10^4$ cm^{-1}. The experimental dependences $J^\omega(T)$ and $\omega_0(T)$ are approximated by (4) and (3)

where A and T' are some coefficients describing the slope and shift of the line. The theoretical dependence is unknown. We can only suppose that the conductivity of the material is hopping. The temperature dependence of the conductivity in glasses is described by the conventional exponential law: $\sigma \propto \exp(-E/k_B T)$ [13]. The investigated range of temperatures is not wide enough to reveal the nonlinear growth of the cut-off frequency. So, the linear approximation used can be considered as a truncated series of the unknown dependence.

Let us consider the temperature dependence of the signal amplitude measured at $\omega > \omega_0$ (Fig. 7). As follows from (1), there is an explicit temperature dependence of the signal arising from the temperature dependence of the diffusion field: $E_D \propto T$. There can also be an implicit function of the temperature resulting from the temperature dependence of material parameters, e.g. photoconductivity σ_0. The linear temperature dependence of σ_0 was assumed above, so the expected dependence of the signal amplitude becomes quadratic:

$$J^\omega = B(T + T')T, \tag{4}$$

where B is a coefficient. One can notice the saturation of the photo-EMF signal at $T > 350$ K. The nature of this saturation is not clear. Perhaps, it is due to temperature dependence of the hole conductivity: in the case of bipolar conductivity the detected signal must decrease since the stationary space-charge gratings formed by electrons and holes are shifted by a half of a spatial period and compensate each other [15].

Utilization of the modified technique for characterization of the as-grown structure in an external ac electric field was not successful [16]. We tried to measure a dependence of the signal amplitude on the electric field strength. No dependences were detected in the fields up to $E_0 = 14$ kV/cm ($\Omega/2\pi \simeq 30$ kHz). This fact is explained by the small value of the diffusion length, which can be estimated as $L_D < k_B T/eE_0 = 18$ nm ($\mu\tau < 1.3 \times 10^{-10}$ cm^2/V). The higher amplitudes of the external field are beyond the breakdown limit, which is about 14 kV/cm for our sample. If the mentioned dependence of the signal on applied field was observed, we could detect the well-known dependence of the conductivity (cut-off frequency) on the frequency of applied field typical for hopping transport: $\omega_0 \propto \sigma \propto \Omega^s$ ($s = 0.8$–0.9 [13]). Such experiments can be considered as the task for further investigation of the effect in other nanostructured materials where transport parameters are more appropriate.

3.3 Polypyrrole in asbestos matrix, $\lambda = 532$ nm

The amplitude of the detected signal in this material is even smaller than that described above. The utilization of the additional signal accumulation and processing in the computer allows us to solve this problem and measure the current with an amplitude of order of 1 fA.

The frequency transfer functions of the non-steady-state photo-EMF signal amplitude are shown in Fig. 8. The growth of the amplitude at low frequencies of the phase modulation ω is present. The frequency-independent region at higher frequencies is not observed because of the limited frequency diapason ($\omega/2\pi < 1$ kHz). The contact photo-EMF, which can also be present, is characterized by the frequency-independent transfer function, so we can state that the observed signal is just the non-steady-state photo-EMF one.

Since the detected signal is very small and direct measurements of the cut-off frequency ω_0 are difficult for this

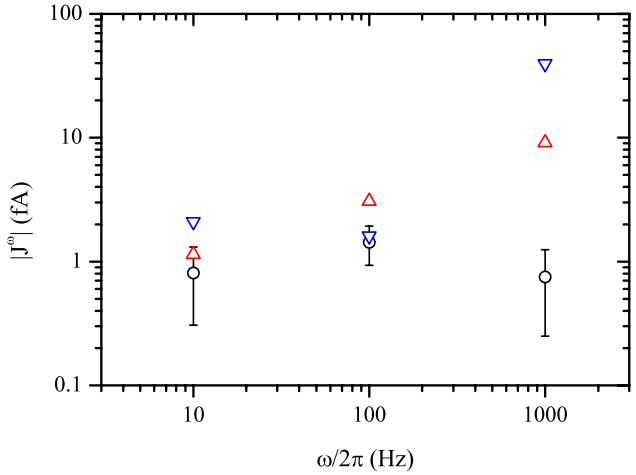

Fig. 8 Frequency transfer functions of the non-steady-state photo-EMF in polypyrrole nanowires within chrysotile asbestos measured for various conditions: ○—standard diffusion regime of the signal excitation, △—diffusion regime with preliminary application of dc voltage $U_{\text{ext}} = +1$ kV, ▽—diffusion regime with preliminary application of dc voltage $U_{\text{ext}} = -1$ kV. $\lambda = 532$ nm, $I_0 = 1.3$ W/cm^2, $K = 11$ μm^{-1}

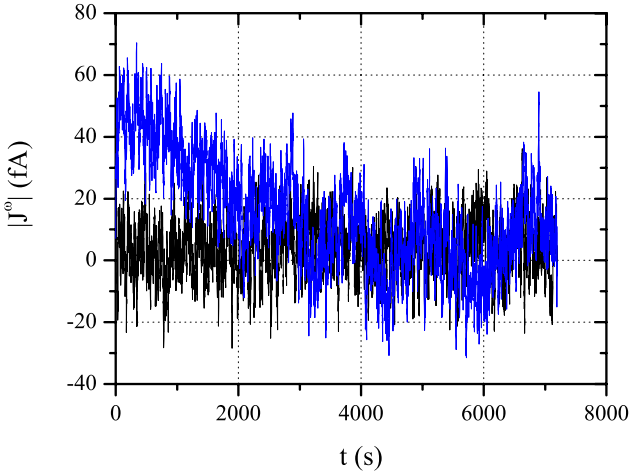

Fig. 9 Time evolution of the detected non-steady-state photo-EMF amplitude. $\lambda = 532$ nm, $I_0 = 1.3$ W/cm^2, $K = 11$ μm^{-1}, $\omega/2\pi = 1$ kHz. The dc electric voltage $U_{\text{ext}} = -1$ kV was applied to the sample before the measurements. The noise level is also shown

material, let us estimate this parameter from the value of the stationary photoconductance measured at direct current: $G = 10^{-9}$–10^{-8} Ω^{-1}. The light penetrates into the medium for a very small distance (the sample is almost black), so let us suppose the effective thickness of the sample with the planar electrodes to be of the order of 10 μm. For this assumption we obtain the estimation for the conductivity $\sigma = GL/S = 10^{-4}$–10^{-3} Ω^{-1} m^{-1}, Maxwell relaxation time $\tau_{\text{M}} = 7$–70 μs ($\epsilon = 800$ [17]), and cut-off frequency $\omega_0/2\pi = 2.2$–22 kHz, which is beyond the frequency range used.

The amplitudes of the detected signal measured without preliminary application of the voltage are stable enough—they do not demonstrate any growth or decay with time. However, such slow evolution is observed in the case with preliminary application of a dc voltage $U_{\text{ext}} = \pm 1$ kV. The time dependence of the non-steady-state photo-EMF amplitude is shown in Fig. 9. We have approximated this dependence by the exponential function and found the time constant $\tau_{\text{E}} = 1900$ s. This value is much greater than the space charge formation time $\tau_{\text{sc}} \sim \tau_{\text{M}}$, so we can state that this decay is not directly associated with the dielectric relaxation processes. It is more likely that the medium slowly relaxes from the state characterized with a larger relation of the photoconductivity σ_0 and dark conductivity σ_{d} to the initial and stable state with a lower relation $\sigma_0/\sigma_{\text{d}}$. Indeed, the amplitude of a stationary space charge field grating recorded in a material with negligible dark conductivity equals $E_{\text{sc}} = -\text{i}mE_{\text{D}}$. The presence of the dark conductivity is equivalent to the decrease of the contrast $m' = m/(1 + \sigma_{\text{d}}/\sigma_0)$ in the process of space-charge recording. As a result, the non-steady-state photo-EMF decreases as well, being directly defined by the amplitude of the electric field grating. Such a behavior can be associated with the fact that polypyrrole exists in two states: oxidized (conducting) and reducing (insulating). The transition from the former to the latter occurs under application of the electric field to the sample [18].

The dependence of signal amplitude on spatial frequency of the interference pattern, i.e. $J^{\omega}(K)$, was also measured for the studied material. There is a linear growth of the signal up to $K \simeq 2$ μm^{-1}, which is due to the increase of the space charge field amplitude $E_{\text{sc}} \propto E_{\text{D}} \propto K$. The signal decreases at $K > 10$ μm^{-1}, which results from 'blurring' of the free-carrier grating [7]. We approximated the experimental dependence by (1) and found the diffusion length as a fitting parameter: $L_{\text{D}} = 0.18$ μm.

4 Conclusion

To summarize, we have investigated the effect of the non-steady-state photo-EMF in porous matrices filled with nanoscaled GaN and polypyrrole. The detected signal revealed a behavior similar to the one typical for wide gap semiconductor crystals. The conductivity of the materials and the diffusion length of photocarriers were estimated from the dependences of the signal on the temporal and spatial frequencies. The temperature dependence of the detected signal in nanostructured GaN and slow evolution of the signal in nanostructured polypyrrole were observed and discussed.

Acknowledgement M.B. and I.S. acknowledge financial support from the Russian Science Support Foundation. The support from the EC-funded project PHOREMOST (FP6/2003/IST/2-511616, Call 5 SRP project 15), Grant No. 07-02-01099 of the Russian Foundation

for Basic Research, and a grant of the President of the Russian Federation (NSh-2184.2008.2) is gratefully acknowledged. The authors thank N.F. Kartenko for help with the XRD characterization of the samples.

References

1. M. Ilegems, J. Cryst. Growth **13–14**, 360 (1972)
2. R.K. Crouch, W.J. Debnam, A.L. Fripp, J. Mater. Sci. **13**, 2358 (1978)
3. N.I. Kuznetsov, A.E. Nikolaev, A.S. Zubrilov, Yu.V. Melnik, V.A. Dmitriev, Appl. Phys. Lett. **75**, 3138 (1999)
4. T.V. Vernitskaya, O.N. Efimov, Russ. Chem. Rev. **66**, 443 (1997)
5. S.M. Ryvkin, *Photoelectric Effects in Semiconductors* (Consultants Bureau, New York, 1964)
6. M.P. Petrov, S.I. Stepanov, A.V. Khomenko, *Photorefractive Crystals in Coherent Optical Systems* (Springer, Berlin, 1991)
7. M.P. Petrov, I.A. Sokolov, S.I. Stepanov, G.S. Trofimov, J. Appl. Phys. **68**, 2216 (1990)
8. P. Levitz, G. Ehret, S.K. Sinha, J.M. Drake, J. Chem. Phys. **95**, 6151 (1991)
9. V.Yu. Davydov, R.E. Dunin-Borkovski, V.G. Golubev, J.L. Hutchison, N.F. Kartenko, D.A. Kurdyukov, A.B. Pevtsov, N.V. Sharenkova, J. Sloan, L.M. Sorokin, Semicond. Sci. Technol. **16**, L5 (2001)
10. L. Bragg, G.F. Claringbull, *Crystal Structure of Minerals* (Bell, London, 1965)
11. N.D. Sobolev, *Introduction to Asbestos Science* (Nedra, Moscow, 1971) (in Russian)
12. I.V. Golosovsky, R.G. Delaplane, A.A. Naberezhnov, Y.A. Kumzerov, Phys. Rev. B **69**, 132301 (2004)
13. N.F. Mott, E.A. Davis, *Electron Processes in Non-crystalline Materials* (Clarendon, Oxford, 1979)
14. S.R. Elliott, *Physics of Amorphous Materials* (Longman, London, 1984)
15. S.I. Stepanov, G.S. Trofimov, Sov. Phys. Solid State **31**, 49 (1989)
16. M. Bryushinin, V. Kulikov, I. Sokolov, Phys. Rev. B **65**, 245204 (2002)
17. A.K. Datta, S. Bhattacherjee, J. Mater. Sci. **21**, 1041 (1986)
18. A.M. Timonov, S.M. Vasilieva, Soros Educ. J. **6**, 33 (2000)